A Mechanistic Study of Halogen Addition and Photoelimination from π-Conjugated Tellurophenes

Elisa I. Carrera,[†] *Anabel E. Lanterna,*[‡] *Alan J. Lough,*[†] *Juan C. Scaiano,**[‡] *and Dwight S. Seferos**[†]

[†]Department of Chemistry, University of Toronto, 80 St. George St., Toronto, Ontario, M5S 3H6, Canada. Email: dseferos@chem.utoronto.ca

[‡]Department of Chemistry and Centre for Catalysis Research and Innovation, University of Ottawa, 10 Marie Curie, Ottawa, Ontario, K1N 6N5, Canada.

Email: scaiano@photo.chem.uottawa.ca

Abstract

The ability to drive reactivity using visible light is of importance for many disciplines of chemistry and has significant implications for sustainable chemistry. Identifying photochemically active compounds and understanding photochemical mechanisms is important for the development of useful materials for synthesis and catalysis. Here we report a series of photoactive diphenyltellurophene compounds bearing electron-withdrawing and electron-donating substituents synthesized by alkyne coupling/ring-closing or palladium-catalyzed *ipso*-arylation chemistry. The redox chemistry of these compounds was studied with respect to oxidative addition and photoelimination of bromine, which is of importance for energy storage reactions involving X_2. The oxidative addition reaction mechanism was studied using density functional theory (DFT), the results of which support a 3-step mechanism involving the formation of an initial η^1 association complex, a monobrominated intermediate, and finally, the dibrominated product. All of the tellurophene derivatives undergo photoreduction using 430 nm,

447 nm or 617 nm light depending on the absorption properties of the compound. Compounds bearing electron-withdrawing substituents have the highest photochemical quantum efficiencies in the presence of an alkene trap, with efficiencies up to 42.4% for a pentafluorophenyl-functionalized tellurophene. The photoelimination reaction was studied in detail through bromine trapping experiments and laser flash photolysis and a mechanism is proposed. The photoreaction, which occurs by release of bromine radicals, is competitive with intersystem crossing to the triplet of the brominated species as evidenced by the formation of singlet oxygen. These findings should be useful for the design of new photochemically active compounds supported by main group elements.

1. Introduction

Light-driven chemical reactions are important for many disciplines of chemistry including synthesis and catalysis due to the relatively low energy input (especially when visible light is used) and the ability to access reaction pathways that are not accessible by thermal activation.[1] Photochemistry has significant implications for sustainable chemistry and renewable energy. The use of light to drive fuel production reactions such has H_2O and HX splitting is becoming increasingly important.[2-6] Several dinuclear late transition metal complexes efficiently photoeliminate halogens, which is the turnover-limiting step in the HX-splitting catalytic cycle. Some of these include Pt-Au,[7] Ir-Au,[8] Au-Au,[9] Pt-Rh,[10] Rh-Rh,[11] and Pt-Pt complexes (Chart 1).[12] This has also been extended to dinuclear systems involving main group elements including Te[13] and Sb,[14] as well as mononuclear systems based on Ni[15] and Pt (Chart 1).[16,17] Photoelimination of HOCl and HOOOH from mononuclear Pt complexes has also been reported.[18,19]

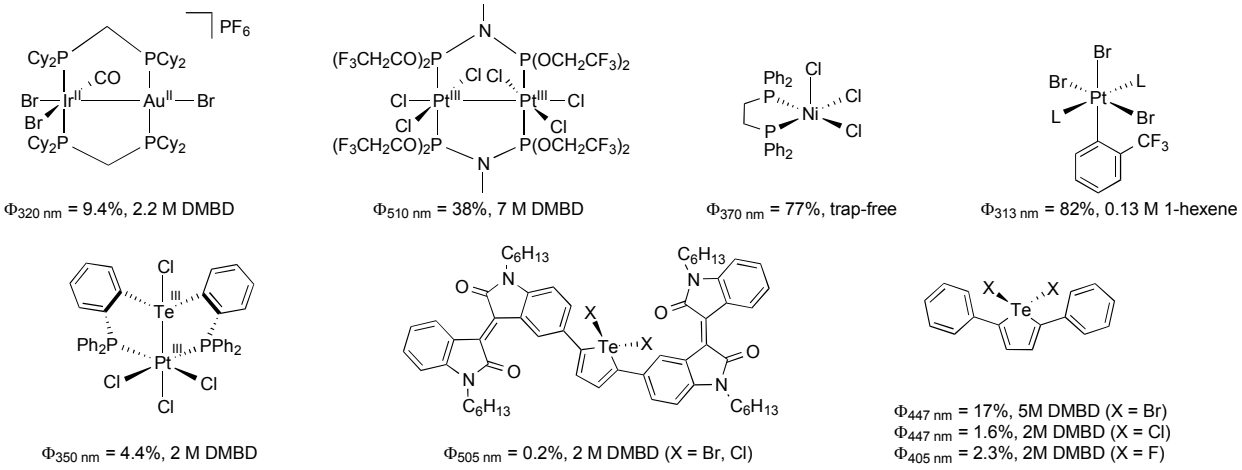

Chart 1. Transition metal complexes and tellurium-containing compounds that undergo halogen photoelimination. Photoelimination quantum yield and halogen traps are indicated below the structure. DMBD = 2,3-dimethyl-1,3-butadiene.

Tellurium-containing π-conjugated molecules and polymers are semi-conducting materials that can be used for organic photovoltaics and organic field effect transistors,[20-31] and as solution and solid-state phosphors.[32-40] The metalloid nature of tellurium necessitates the development of new synthetic pathways to access novel tellurium-containing heterocycles. Some recent examples include Te-B heterocycles,[41-43] 1,4-diphenyl-1-telluro-1,3-butadiene incorporated in a dibenzobarrelene skeleton,[39] a silylated oxatelluronium halide (a five-membered heterocycle containing a Te-O bond),[44] and mercaptobenzotellurazoles,[45] to name a few.

Fundamental studies on the reactivity of tellurium-containing compounds are important for the discovery of new useful transformations utilizing these compounds. Te(II)/Te(IV) redox chemistry with halogens and other oxidants has been known for quite some time. 3-center-4-electron X-Te-X bonds are formed in the presence of dihalogens or dihalogen sources where the Te(IV) atom is hypervalent (Chart 2).[20,46-51] This leads to significant changes in the optoelectronic properties of the compound. Te(II) can also be oxidized to the telluroxide or tellurone using hydrogen peroxide or organic peroxides such as *m*-chloroperoxybenzoic acid (mCPBA; Chart 2).[38,39,52] In some cases, this oxidative chemistry is thermally or electrochemically reversible. Recently, Dutton and coworkers reported the oxidation of 2,5-diphenyltellurophene by other iodine-based oxidants such as $PhI(OTf)_2$ and PhI(OTf)(OAc), yielding the diacetate and the mixed acetate/triflate ligated tellurophenes, respectively.[53] A rather unexpected C-H to C-N bond metathesis reaction was discovered when an analogous iodobenzene complex bearing two 4-dimethylaminopyridine (DMAP) groups was used as the oxidant, resulting in DMAP functionalization at the 3 position of the tellurophene ring (Chart 2).

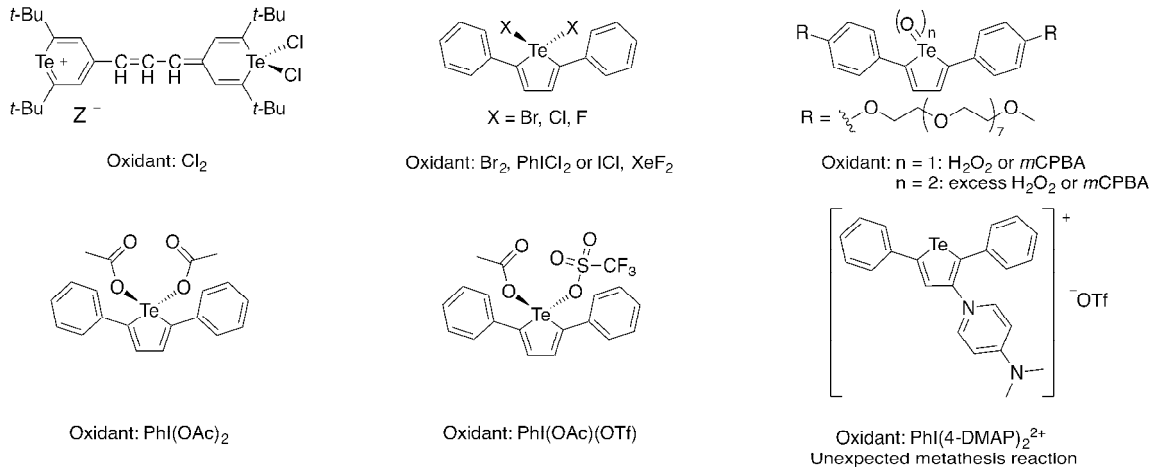

Chart 2. Tellurium-containing heterocycles prepared with different oxidants.

We recently discovered that visible light will drive photoreduction of Te(IV) within π-conjugated tellurophenes. The conjugated nature of the tellurophene allows for the use of visible light to drive reactivity. Furthermore, the ease of tunability of the substituents at the 2 and 5 positions allows for tailoring of the optical properties and hence irradiation wavelength. We have previously shown that irradiation with green light can induce photoelimination of bromine and chlorine from isoindigo-functionalized tellurophenes (Chart 1), however the photochemical quantum yields of this system were limited due to unfavorable excited state electronics.[50] Earlier this year we reported an eighty-five fold improvement in the quantum efficiency (up to 17%) for 2,5-diphenyltellurophene (Chart 1).[51] However, the mechanism of this reaction, and its optimization are still unresolved. Here, we report a series of substituted diphenyltellurophenes, focusing on the effect of electron-donating groups (EDGs) and electron-withdrawing groups (EWGs) on the structure, properties and photochemistry of these compounds. We provide mechanistic studies of both the oxidative addition and photoelimination reactions through the use of DFT, halogen-trapping experiments, and laser flash photolysis (LFP). The optimized

structures have photochemical quantum yields that exceed 40%, do not contain transition metals, and photoelimination occurs solely from the Te(IV) center.

2. Results and Discussion

2.1. Molecule Design and Synthesis. 2,5-Diphenyltellurophenes can be modified with a range of functional groups to give diphenyltellurophene (**PT-R**) compounds with varying degrees of electron-donating or electron-withdrawing character (Chart 3). The electron-withdrawing substituents chosen were 4-trifluoromethylphenyl (**PT-CF_3**), 4-cyanophenyl (**PT-CN**), and pentafluorophenyl (**PT-C_6F_5**) groups. The electron-donating substituents chosen were 4-*tert*-butylphenyl (**PT-*t*Bu**), 4-*tert*-butoxyphenyl (**PT-O*t*Bu**), and 4-(*N*,*N*-diethylamino)phenyl (**PT-NEt_2**) groups. We also chose to study an asymmetric push-pull type tellurophene bearing both an electron-donating 4-(*N*,*N*-dibutylamino)phenyl group and an electron-withdrawing 4-nitrophenyl group (**PT-NO_2-NBu_2**).

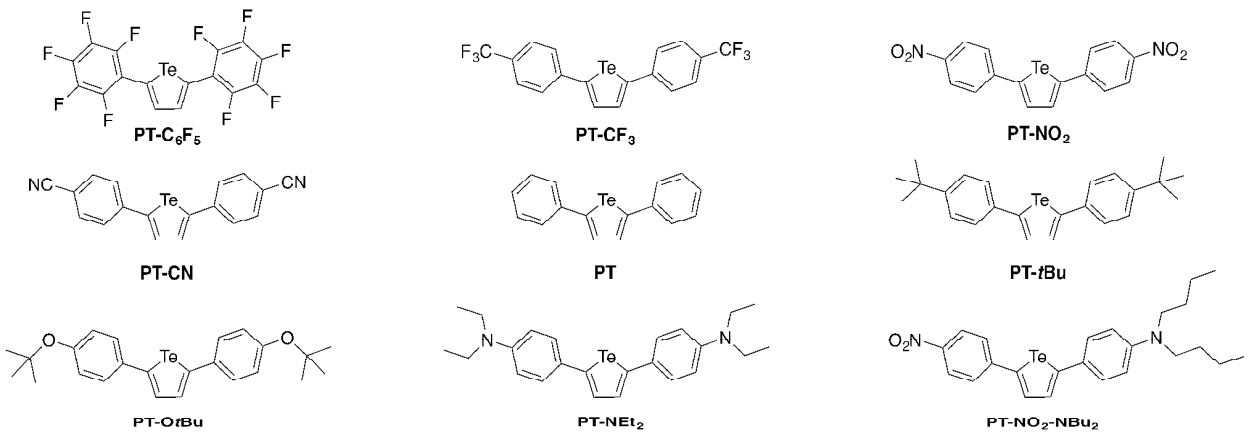

Chart 3. Chemical structures of **PT** derivatives.

The compounds were synthesized by one of two routes: a Glaser Hay alkyne coupling/ring closing procedure (Scheme 1a),[54,55] or *ipso*-arylative cross-coupling (Scheme 1b).[56,57] The alkyne

coupling/ring closing procedure involves copper-catalyzed homocoupling of substituted terminal alkynes to form the disubstituted diacetylene precursor (compounds **1** and **2**). The precursor is then introduced into a suspension of sodium telluride (generated by reduction of tellurium powder with sodium borohydride), to give the ring-closed tellurophene product. This procedure worked well for **PT**, **PT-CF_3** and **PT-*t*Bu**, however it was less successful for some of the other compounds such as **PT-NEt_2**, and **PT-NO_2**, due to poor yield, poor solubility, decomposition, or because the alkyne starting material was not commercially available. Recently, Grubbs and coworkers reported that palladium-catalyzed *ipso*-arylation chemistry will couple aryl substituents onto tellurophenes and benzotellurophenes to give polymers and small molecules.[25,26] We adopted this chemistry to synthesize the remaining tellurophene compounds. The previously reported synthesis of the tellurophene *ipso*-arylation coupling partner, 2,5-bis[(diphenyl)hydroxymethyl]tellurophene (**4**), however, was modified in our study. Specifically, the diacetylene precursor **3** was synthesized via homocoupling of the commercially available alkyne, 1,1-diphenyl-2-propyn-1-ol, and then subjected to the ring-closing conditions discussed earlier to produce **4**. The tellurophene compounds **PT-O*t*Bu**, **PT-CN**, and **PT-C_6F_5** were then synthesized via *ipso*-arylation cross-coupling of **4** with the appropriate aryl bromide or iodide. Unfortunately, the *ipso*-arylation approach was also unsuccessful for the direct synthesis of **PT-NEt_2** and **PT-NO_2-NBu_2**. In order to synthesize these compounds, **PT-NO_2** was prepared via *ipso*-arylation, and one or both of the nitro groups were reduced followed by *N*-alkyl substitution using the appropriate alkyl iodide (Scheme 1c).

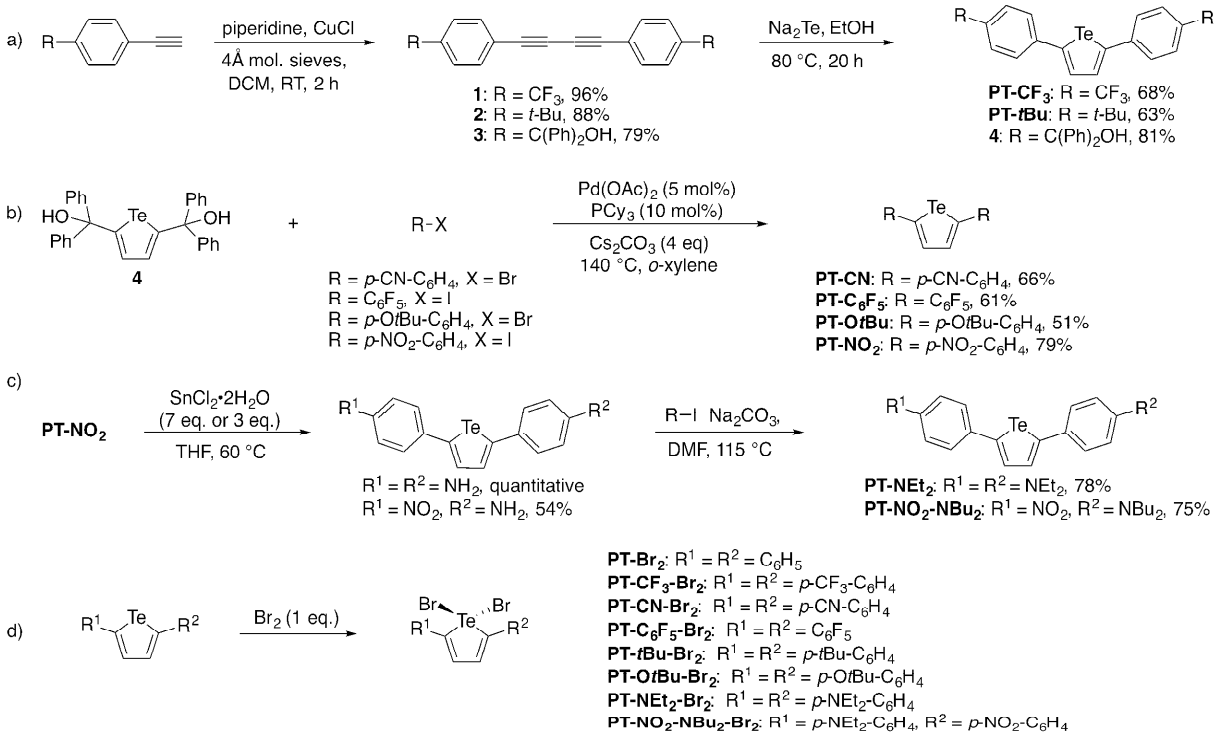

Scheme 1. a-c) Synthetic routes for the preparation of **PT-R** compounds. d) Preparation of **PT-R-Br$_2$** compounds.

2.2. Optical Properties of PT-R Compounds and Their Te(IV) Adducts. Aside from **PT-NEt$_2$** and **PT-NO$_2$-NBu$_2$**, all of the tellurophene compounds have similar optical absorption maxima (λ_{max}), ranging from 330 nm to 365 nm in chloroform with ~ 10^4 M^{-1} cm^{-1} molar absorptivity (Table 1). The λ_{max} of **PT-NEt$_2$** and **PT-NO$_2$-NBu$_2$** appear at longer wavelengths (408 nm and 466 nm, respectively, in toluene). The relatively low energy absorption of **PT-NO$_2$-NBu$_2$** is characteristic of push-pull type chromophores. Oxidative addition of bromine to the tellurium center leads to a lower energy λ_{max} for all of the compounds. Increasing titration with Br_2 in $CHCl_3$ (or toluene for **PT-NEt$_2$-Br$_2$** and **PT-NO$_2$-NBu$_2$-Br$_2$**) leads to a decrease in the absorption corresponding to the parent tellurophene accompanied by an increase in absorption at

both higher and lower energy wavelengths (Figure 1; Figure S1, Supporting Information). Clear isosbestic points (IPs) indicate clean conversion to the brominated compound. The red-shift in the lower energy λ_{max} of the brominated compound compared to the parent compound is much more pronounced for compounds bearing EDGs (103, 111, and 156 nm for **PT-*t*Bu-Br$_2$**, **PT-O*t*Bu-Br$_2$**, and **PT-NEt$_2$-Br$_2$**, respectively) than those bearing EWGs (52, 68, and 78 nm for **PT-CN-Br$_2$**, **PT-CF$_3$-Br$_2$**, and **PT-C$_6$F$_5$-Br$_2$**, respectively). A red-shift of 100 nm is observed for **PT-NO$_2$-NBu$_2$-Br$_2$**. NMR spectroscopy experiments were carried out with each tellurophene compound in $CDCl_3$ (or deuterated toluene for **PT-NEt$_2$** and **PT-NO$_2$-NBu$_2$**). In each case, complete conversion to the brominated product was achieved using one equivalent of Br_2. The brominated compounds (**PT-R-Br$_2$**) were also synthesized on a preparative scale and isolated (see Experimental Section, Supporting Information for more detail). Additionally, the structures of **PT-*t*Bu-Br$_2$**, **PT-O*t*Bu-Br$_2$**, **PT-CF$_3$-Br$_2$**, and **PT-C$_6$F$_5$-Br$_2$** were confirmed by X-ray crystallography (Figure 2).

Table 1. Optical Absorption Properties of the Tellurophene Compounds in $CHCl_3$.

	λ_{max} (nm)		ε (M^{-1} cm^{-1})		$\Delta\lambda_{max}$ (nm)	$\Delta\varepsilon$ (M^{-1} cm^{-1})
	parent	+ Br_2	parent	+ Br_2		
PT-NEt$_2$	408[a]	564[a]	3.31×10^4	1.52×10^4	156	-1.79×10^4
PT-O*t*Bu	354	465	2.56×10^4	9.70×10^3	111	-1.59×10^4
PT-*t*Bu	349	452	2.33×10^4	8.54×10^3	103	-1.48×10^4
PT	342	433	2.24×10^4	6.34×10^3	91	-1.61×10^4
PT-CN	365	417	3.12×10^4	1.11×10^4	52	-2.01×10^4
PT-CF$_3$	346	415	2.13×10^4	6.96×10^3	69	-1.43×10^4
PT-C$_6$F$_5$	330	408	2.52×10^4	9.29×10^3	78	-1.59×10^4
PT-NO$_2$-NBu$_2$	477[a]	566[a]	2.61×10^4	2.06×10^4	89	-5.50×10^3

[a]Measured in toluene.

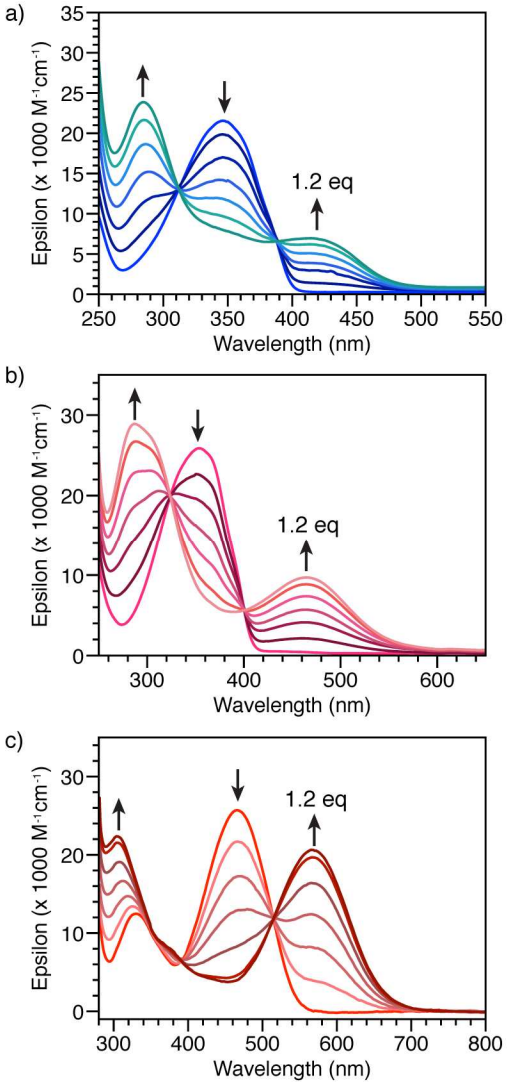

Figure 1. Optical absorption spectra of bromine titration experiments for a) **PT-CF$_3$** ($CHCl_3$), b) **PT-O*t*Bu**, ($CHCl_3$), and c) **PT-NO$_2$-NBu$_2$** (toluene).

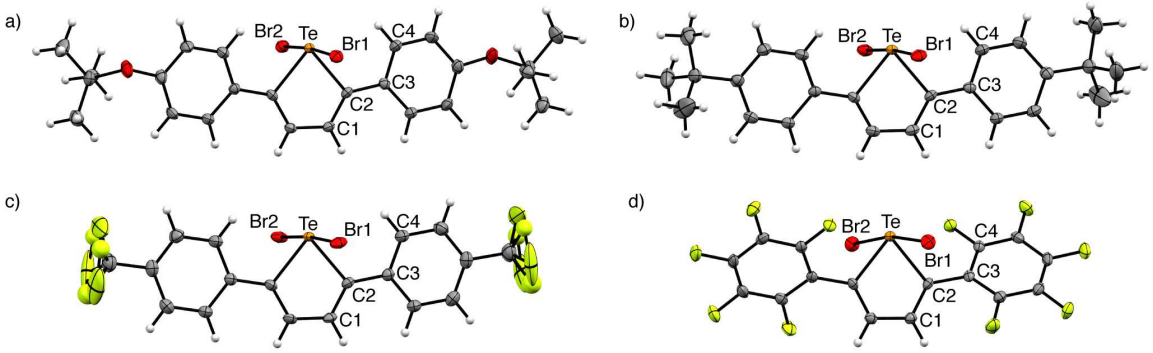

Figure 2. Displacement ellipsoid plots of a) **PT-O*t*Bu-Br$_2$**, b) **PT-*t*Bu-Br$_2$**, c) **PT-CF$_3$-Br$_2$** (the F atoms are disordered over two sets of sites with the minor component shown as small spheres) and d) **PT-C$_6$F$_5$-Br$_2$** shown at 50% probability.

2.4. Computational Modeling. *2.4.1. Excited State Properties.*

Time dependent (TD) DFT calculations were carried out on the gas-phase optimized structures to determine the calculated absorption spectrum of each compound and the nature of the associated transitions. Overall, the calculations predict the absorption spectra quite well in terms of shape and magnitude of the extinction coefficient, however the calculated spectra are overall red-shifted compared to the experimental spectra (Figure S2, Supporting Information). For all of the compounds (including the brominated compounds), the lowest energy transition with significant oscillator strength is HOMO to LUMO in nature. The calculations predict a decreased HOMO–LUMO energy gap upon bromination (Figure S3, Supporting Information) that is consistent with the experimental spectra. Visualization of the frontier molecular orbitals of the non-brominated tellurophenes show that this transition is a delocalized π–π^* transition, while the HOMO to LUMO transition in the brominated compounds has charge-transfer character from a delocalized state onto the dibromotellurophene unit (Figure 3). The LUMO has significant

electron density within the antibonding Te–Br orbitals. Excitation into this state should promote photoelimination of bromine.

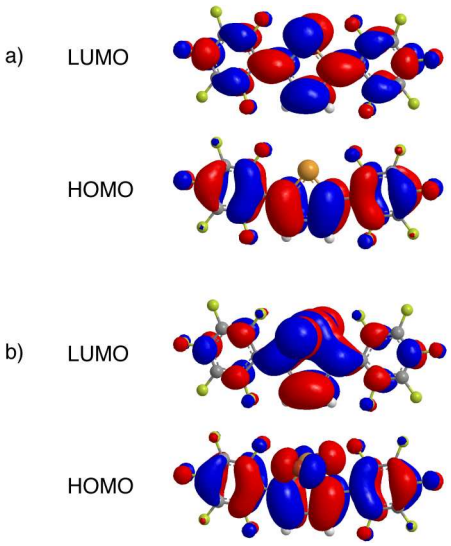

Figure 3. Molecular orbital diagrams for a) **PT-C_6F_5** and b) **PT-C_6F_5-Br_2**.

2.4.2. Oxidative Addition Mechanistic Study. It is important to note that the mechanism of bromine addition to tellurophene is unknown. Detty and coworkers proposed two possible mechanisms for this reaction involving other organotellurium compounds.[48] Stopped-flow kinetics experiments revealed three distinct processes: an initial "fast" reaction followed by two slower ones. The "fast" reaction was attributed to the formation of an initial association complex between molecular bromine and the tellurium atom, which was speculated to be in either an "end-on" η^1 or "edge-on" η^2 fashion. From here, the addition of Br_2 to tellurium could either occur via a concerted mechanism (from an η^2 association complex; Scheme 2a) or a dissociative mechanism (from an η^1 association complex) with the formation of an ionic intermediate (Scheme 2b).

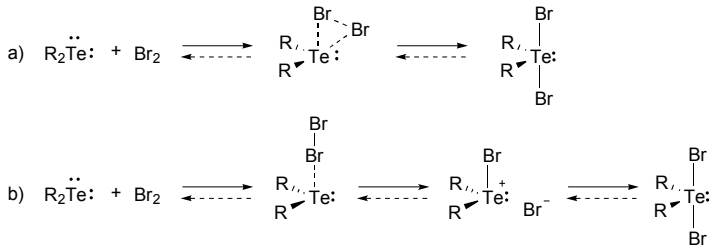

Scheme 2. Possible mechanisms for oxidative addition of molecular bromine to organotellurium compounds: a) a concerted mechanism involving an η^2 association complex; or b) a dissociative mechanism involving an η^1 association complex and an ionic intermediate. Adapted and simplified from ref. 48.

Here, we used DFT geometry optimizations to model molecular bromine in close proximity to diphenyltellurophene. Three different minima were found depending on the starting positions of the molecules in the input file. One structure resembles an "end-on" η^1 association complex (**Int1**), one resembles a monobrominated species suggestive of an ionic intermediate (**Int2**), and the last structure resembles that of the brominated product (**PT-Br$_2$**). Frequency calculations verify that each of these structures are minima. Attempts to locate an optimized structure involving an "edge-on" η^2 association complex were unsuccessful.

Synchronous transit-guided quasi-Newton[58,59] (STQN) calculations were performed to locate a transition state connecting **Int1** with **Int2** (**TS1-2**), and **Int2** with **PT-Br$_2$** (**TS2-P**). The transition state calculations were successfully optimized to maxima, resulting in structures with an intermediate geometry between the geometries of the two minima that they connect. To verify that **TS1-2** and **TS2-P** are the true transition state structures, frequency calculations and intrinsic reaction coordinate (IRC)[60] calculations were performed. The frequency calculations predict one negative frequency, which is expected for a transition state. The vibrations associated with this negative frequency involve motions of the bromine atoms in a manner that

supports a transition from **Int1** to **Int2** in the case of **TS1-2**, and from **Int2** to **PT-Br$_2$** in the case of **TS2-P**. IRC calculations follow the reaction pathway from the transition state to the minima and can confirm whether a calculated transition structure truly connects the two minima of interest. IRC calculations from **TS1-2** and from **TS2-P** indeed led to structures resembling **Int1**, **Int2**, and **PT-Br$_2$** as expected (Figure S4 and S5, Supporting Information), and geometry optimizations from the final IRC structures led to the identical minimum energy structures that were obtained from the geometry optimizations of Br_2 in close proximity to **PT** discussed earlier. Although attempts to locate a minimum energy η^2 association complex were unsuccessful, attempts were also made to locate a transition state with this structure. A maximum was successfully located, however the molecular distortion associated with the negative frequency does not involve the bromine atoms and thus does not support a connection to the product structure. Furthermore, IRC calculations from this structure were unsuccessful. Thus, no evidence for a concerted oxidative addition mechanism was found. Finally, an attempt to connect **Int1** directly to **PT-Br$_2$** through a single transition state was also made. The calculation successfully optimized to a maximum structure, however this structure was identical to **TS1-2**, and the IRC calculation led to structures resembling **Int1** and **Int2** rather than **PT-Br$_2$**. This confirms that **TS1-2** does not connect **Int1** directly to the product (**PT-Br$_2$**), but instead to the monobrominated intermediate **Int2**. Overall, the results of the DFT calculations support a three-step oxidative addition mechanism involving the sequential formation of an initial η^1 association complex, a monobrominated intermediate, and finally the brominated product (Scheme 2b). Scaled frequency calculations and high accuracy SPE calculations were performed for all of the optimized structures in order to determine accurate zero-point-corrected energies. The calculations were also repeated using a chloroform polarizable continuum model (PCM). The

geometries obtained with the chloroform model are only slightly different than the gas phase geometries. The zero-point corrected energies obtained from the calculations with a solvent model were used to produce a reaction pathway energy diagram for the oxidative addition process (Figure 4). Although the geometries calculated with a solvent model are similar to the gas phase optimized geometries, the energies of all structures are stabilized when the chloroform model is applied. A much larger degree of stabilization is predicted for the monobrominated intermediate **Int2** and the transition states connecting **Int2** to its reactant and product (Figure S6, Supporting Information).

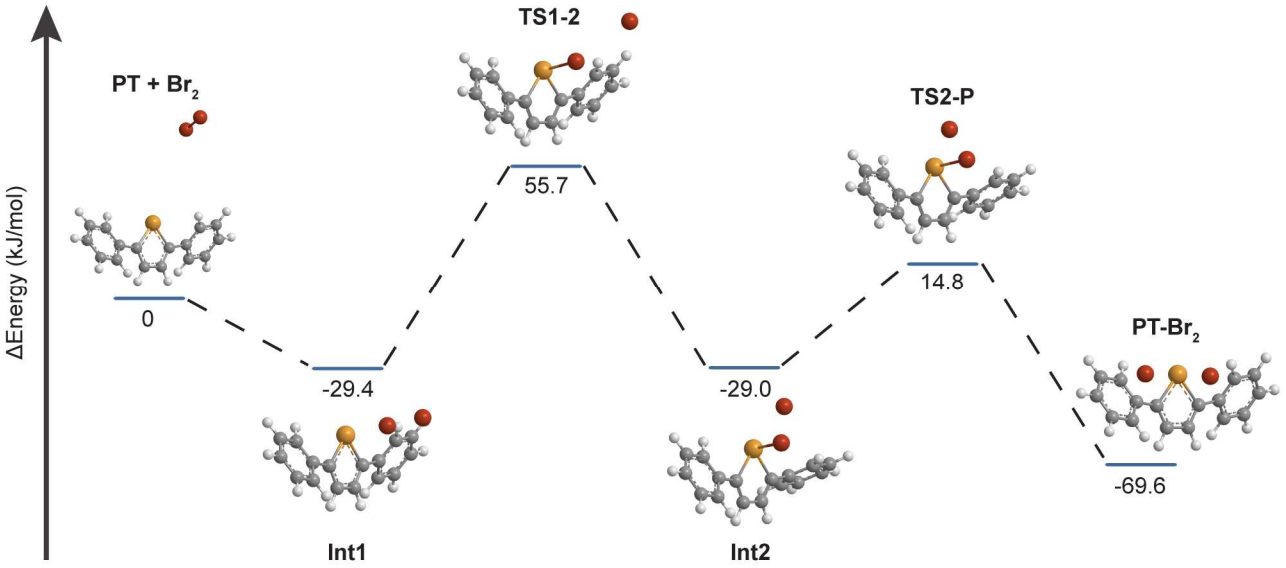

Figure 4. DFT-calculated reaction pathway energy diagram for the oxidative addition of bromine to **PT**, calculated with a $CHCl_3$ PCM.

2.5. Photochemistry. *2.5.1. Photolysis Experiments.* Photolysis experiments were carried out on the brominated compounds by irradiating at the lowest energy absorption band. The reactions were monitored using optical absorption spectroscopy. We will first discuss **PT-Br$_2$** and the compounds bearing EDGs. Irradiation of **PT-Br$_2$**, **PT-*t*Bu-Br$_2$** and **PT-O*t*Bu-Br$_2$** at 447 nm in the presence of 1 M 2,3-dimethyl-1,3-butadiene (DMBD) halogen trap led to spectral changes

consistent with conversion back to the parent compounds. A comparison of the photolysis product spectra with those of each of the parent compounds showed some differences, specifically a slight blue-shift in both the λ_{max} and isosbestic points (Figure S7, Supporting Information). This is attributed to the formation of decomposition products during photolysis. Based on the magnitude of the difference between the photolysis product spectrum and the parent spectrum, the amount of decomposition is more significant for compounds with stronger EDGs. Increasing the DMBD concentration to 3 M, however, leads to clean conversion of **PT-Br$_2$** to **PT**, and only slight decomposition in the case of **PT-*t*Bu-Br$_2$** (Figure S8, Supporting Information) and **PT-O*t*Bu-Br$_2$** (Figure 5a). Photolysis was complete within 5, 16, and 40 seconds for **PT-Br$_2$**, **PT-*t*Bu-Br$_2$**, and **PT-O*t*Bu-Br$_2$**, respectively, showing that the irradiation time required to achieve complete conversion increases with donating strength. This is consistent with strong electron-donating character hindering the reductive elimination process. Due to the low energy absorption of **PT-NEt$_2$-Br$_2$** and **PT-NO$_2$-NBu$_2$-Br$_2$** red-orange (617 nm) light was used for irradiation. For the strongly-donating **PT-NEt$_2$-Br$_2$**, photolysis was complete within 6 minutes and the optical absorption spectrum is indicative of the formation of decomposition products (Figure S8, Supporting Information), consistent with the other compounds bearing EDGs. Interestingly, much longer irradiation time was required for **PT-NO$_2$-NBu$_2$-Br$_2$** (160 minutes), and the optical absorption spectrum indicates an even greater amount of decomposition, as evidenced by the blue-shifted λ_{max} and isosbestic points.

We next discuss the compounds bearing EWGs. Irradiation of **PT-CF$_3$-Br$_2$** (Figure 5c), **PT-CN-Br$_2$**, and **PT-C$_6$F$_5$-Br$_2$** (Figure S8, Supporting Information), at 430 nm in the presence of 3 M DMBD led to complete conversion back to the respective parent compounds within a few

seconds. For these compounds the photolysis product optical absorption spectra are identical to the spectra of the parent compounds and there is no evidence of decomposition.

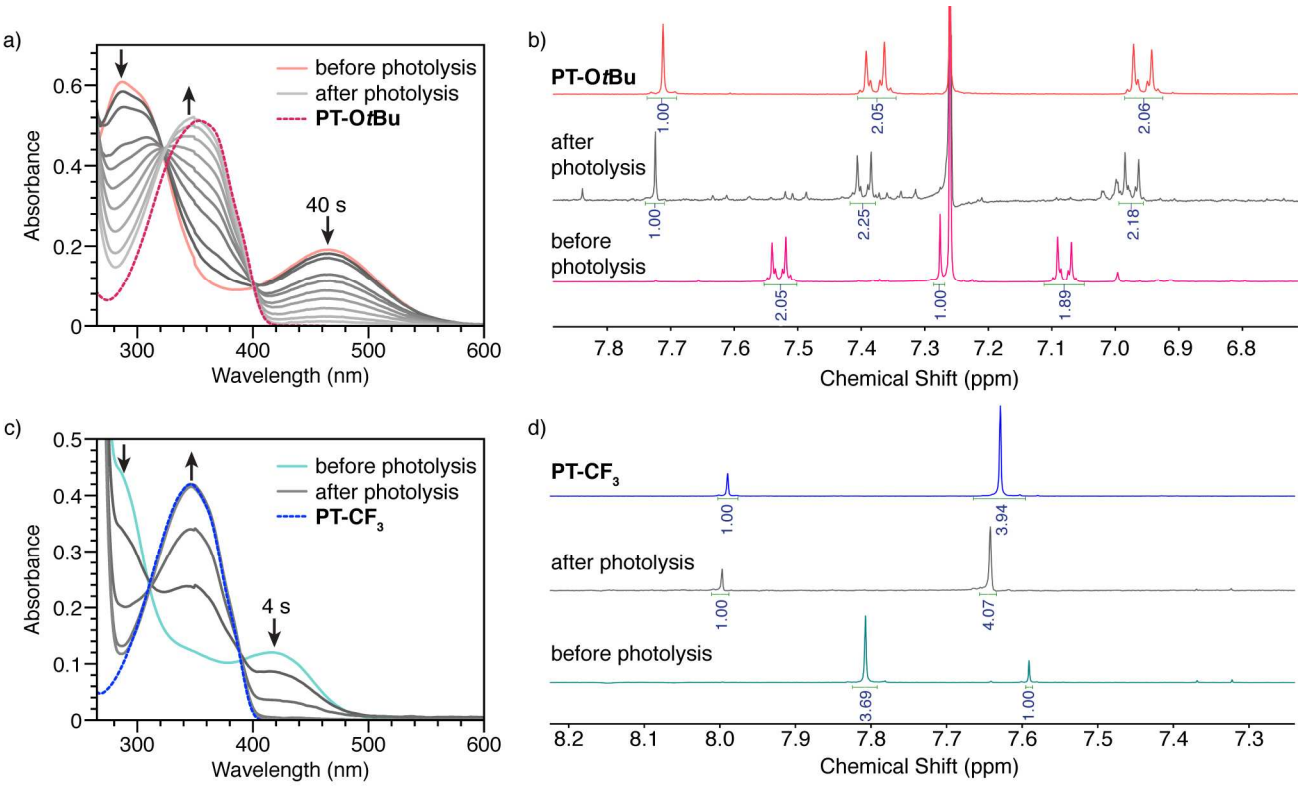

Figure 5. Optical absorption and ^{1}H NMR spectra showing the photolysis of **PT-O*t*Bu-Br$_2$** (a-b) and **PT-CF$_3$-Br$_2$**, (c-d).

All photolysis reactions were also characterized by NMR spectroscopy. Consistent with the optical absorption spectra, some decomposition is observed during the photolysis of **PT-*t*Bu-Br$_2$** (Figure S9, Supporting Information) and **PT-O*t*Bu-Br$_2$** (Figure 5b) indicated by the presence of additional peaks in the aromatic region, as well as some discrepancy in the integration of the tellurophene proton signals. Photolysis of **PT-NEt$_2$-Br$_2$** and **PT-NO$_2$-NBu$_2$-Br$_2$** leads to decomposition and no evidence of the brominated starting materials (Figure S10 and S11, Supporting Information). On the other hand, photolysis of **PT-CF$_3$-Br$_2$** (Figure 5d), **PT-CN-Br$_2$**,

and **PT-C_6F_5-Br_2** (Figure S12 and S13, Supporting Information) leads to complete conversion to the parent compounds with no evidence of additional product formation in the NMR spectra, confirming that these reactions are quite efficient and free of side reactions. The tellurophene compounds demonstrate high thermal stability, thus thermal reduction is of no concern in the photolysis experiments (see Supporting Information for thermal control experiments).

2.5.2. Photochemical Quantum Yield Determination. The efficiencies of photoelimination were evaluated by determining the photochemical quantum yield, Φ_P, using potassium ferrioxalate actinometry (Table 2).[61-63] **PT-Br_2** has a photochemical quantum yield of 8.5% at 2 M DMBD concentration.[51] The incorporation of EDGs onto the phenyl ring reduces the quantum yield of photoelimination for **PT-*t*Bu-Br_2** (1.61 ± 0.04%) and **PT-O*t*Bu-Br_2** (0.44 ± 0.01%). On the contrary, the incorporation of EWGs increases the quantum yield for **PT-CN-Br_2** (14.7 ± 0.3%), **PT-CF_3-Br_2** (19.2 ± 0.7%) and **PT-C_6F_5-Br_2** (23.6 ± 0.7%). These observations are consistent with the EWGs facilitating photoelimination by making Te more electropositive.

Table 2. Photochemical Quantum Yield for Photoelimination of Bromine from PT derivatives.

	[DMBD] (M)	Φ_P (%)[a]	Std. Dev. (%)	Relative Φ_P
PT-NEt_2-Br_2	2	--	--	0.007[b]
PT-O*t*Bu-Br_2	2	0.44	0.01	0.05
PT-*t*Bu-Br_2	2	1.61	0.04	0.2
PT-Br_2	2	8.5	0.3	1
PT-CN-Br_2	2	14.7	0.3	1.7
PT-CF_3-Br_2	2	19.2	0.7	2.3
PT-C_6F_5-Br_2	1	17.6	0.5	
	2	23.6	0.7	2.8
	3	31.3	0.2	
	4	36.6	0.5	
	5	42.4	0.4	
PT-NO_2-NBu_2-Br_2	2	--	--	0.0002[b]

[a]Determined by potassium ferrioxalate actinometry.
[b]Estimated from output of light source and change in concentration for a given irradiation period.

The quantum yields for **PT-NEt$_2$-Br$_2$** and **PT-NO$_2$-NBu$_2$-Br$_2$** could not be determined since the irradiation wavelength (617 nm) is beyond the absorption range of the actinometer. However, the radiant power of the light sources (from manufacturer specifications) and the change in concentration for a given irradiation period were considered in order to draw a relative comparison (see Supporting Information for detailed calculation). From these calculations, bromine photoelimination from **PT-NEt$_2$-Br$_2$** and **PT-NO$_2$-NBu$_2$-Br$_2$** is approximately 0.007 and 0.0002 times less efficient than from **PT-Br$_2$**, respectively (Table 2).

The extremely poor efficiency for **PT-NO$_2$-NBu$_2$-Br$_2$** is somewhat surprising. It might be expected that **PT-NO$_2$-NBu$_2$-Br$_2$** would have similar photochemical behavior to the unsubstituted **PT-Br$_2$** due to a cancelling effect of the strong EDG and EWG on either end of the molecule. Rationalization of the unprecedented low efficiency was attempted based on electrostatic potential (ESP) maps from the DFT calculations. The ESP maps of **PT-Br$_2$**, **PT-NEt$_2$-Br$_2$**, and **PT-C$_6$F$_5$-Br$_2$** show increasing positive ESP at Te with increasing electron-withdrawing character (Figure 6a). The incorporation of both a strong EWG and a strong EDG onto each end of the molecule does indeed have a cancelling effect on the ESP at Te, resulting in an ESP map for **PT-NO$_2$-NBu$_2$-Br$_2$** that is quite similar to that of **PT-Br$_2$**. Thus, the sluggish photochemical behavior cannot be explained by an ESP argument. Instead, analysis of the MO diagrams provides more insight into this behavior. The MO diagrams for **PT-NO$_2$-NBu$_2$-Br$_2$** display the typical charge transfer character of push-pull chromophores. Thus, rather than being localized only on the dibromotellurophene ring, as is the case for the other derivatives, the electron density in the LUMO is delocalized across both the dibromotellurophene ring and the NO$_2$-substituted phenyl ring (Figure 6b). This decreases the Te-Br anti-bonding character in the

LUMO compared to the other derivatives, which likely explains the unexpected poor efficiency observed for this compound.

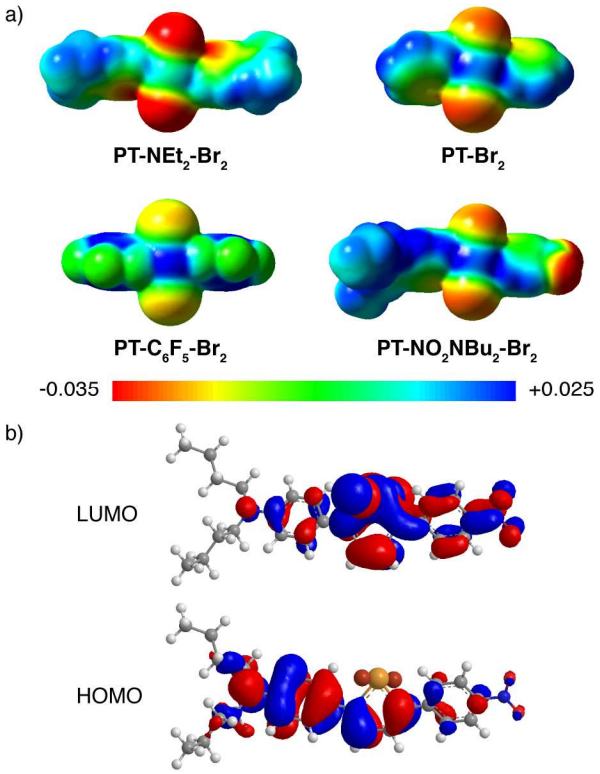

Figure 6. a) ESP maps of indicated compounds. b) MO diagrams for **PT-NO_2-NBu_2-Br_2**.

Finally, a trap-dependent quantum yield study was carried out for the most efficient compound, **PT-C_6F_5-Br_2** (Table 2). A linear dependence of quantum yield on trap concentration is observed (Figure S14, Supporting Information), with an impressive value of 42.4 ± 0.4% at 5 M DMBD concentration, the best value for a tellurophene reported to date.

2.6. Mechanistic Details of Tellurophene Photochemistry. *2.6.1. Halogen Trapping Experiments.* To gain insight into the photoelimination mechanism, the identity of the liberated bromine species was investigated by characterizing the trapped products. For these experiments, **PT-C_6F_5-Br_2** was the reactant and 2,3-dimethyl-2-butene (DMB) was used as the trap in order to simplify the number of possible trap products. Molecular bromine would be expected to yield

the Br_2 addition product 2,3-dibromo-2,3-dimethylbutane (DMB-Br_2).[64] Thus, if bromine is reductively eliminated as Br_2, (or leads to the formation of Br_2) this would be the only expected trap product. On the other hand, if bromine is released as two bromine radicals ($Br^{\bullet}$), then reaction of one $Br^{\bullet}$ with DMB would be expected to yield HBr and an allylic radical ($DMB^{\bullet}$), which could then react with the second $Br^{\bullet}$ to produce 1-bromo-2,3-dimethyl-2-butene (DMB-Br).[65] Additionally, the HBr produced from this process could also react with DMB to give the HBr addition product 2-bromo-2,3-dimethylbutane (DMB-HBr).[66] Evidence of both the allylic bromination product DMB-Br (singlet at δ = 4.08 ppm) and the Br_2 addition product DMB-Br_2 (singlet at δ = 2.03 ppm; Figure S15a, Supporting Information) are present after photolysis. The ratio of DMB-Br to DMB-Br_2 is approximately 6:1 suggesting that the dominant pathway involves $Br^{\bullet}$. Compared to the integration of **PT-C_6F_5**, the yields are 39% DMB-Br and 7% DMB-Br_2, which suggests that 54% of the liberated bromine is consumed in additional processes. Surprisingly, there is no evidence of DMB-HBr in the ^{1}H NMR spectrum despite the fact that DMB-Br is formed in 39% yield. However, there are several other significant peaks in the alkyl region after photolysis with unknown identities (singlets at δ = 1.93, 1.86, 1.85 and 1.49 ppm; Figure S15b, Supporting Information), which could account for the remaining trapped bromine.

In order to further investigate bromine trapping, GC-MS analysis was carried out on the photolyzed samples. The trap products DMB-Br_2 and DMB-Br were prepared separately for comparison (Figure S16-S17, Supporting Information). Evidence of both DMB-Br_2 (RT = 6.05 min) and DMB-Br (RT = 4.94 min) is observed in the photolyzed sample (Figure S18, Supporting Information). However, additional product(s) with a retention time of 4.92 min coeluted with DMB-Br. An analysis of the chromatogram peak at 4.94 min shows the expected

mass for DMB-Br, with two equal intensity peaks at m/z of 162 and 164. Analysis of the same chromatogram peak at 4.92 min also shows two peaks of roughly equal intensity in the MS, however these are shifted to m/z of 165 and 167. While the retention time and MS pattern of the unidentified product(s) are suggestive of a monobrominated alkane, extensive efforts to determine the identity of the compound(s) were unsuccessful (for further discussion, see the Supporting Information).

The expected retention time for **PT-C_6F_5** is 12.71 min, and only a slight difference in retention time is observed for the photolysis product (12.76 min) with an identical fragmentation pattern (Figure S19, Supporting Information). Comparing the integration of the DMB-Br_2 peak in the GC with the **PT-C_6F_5** peak gives a ratio of 0.063:1, corresponding to a 6.3% yield of DMB-Br_2 (Figure S20, Supporting Information). This is in excellent agreement with the yield determined by NMR integration. Comparing the integration of the peak at 4.92 min (which contains both DMB-Br and the other product(s)) with that of **PT-C_6F_5** gives a ratio of 0.77:1, corresponding to a 77% yield of these products. This is roughly twice the NMR determined yield of DMB-Br suggesting a 1:1 ratio of DMB-Br to the unidentified trap product(s). The total yield of the discussed products from the GC analysis is approximately 83%. There are a few other low intensity peaks in the GC ranging from RT of 6.56 to 8.67 min, which likely account for the remainder of the trapped bromine.

Although the identity of the additional major trap product(s) remains unclear, the results of the trapping experiments show that the photoelimination reaction occurs predominantly by elimination of radical bromine. The Br_2 addition product, which is formed in very small quantities, could be formed by Br_2 produced by combination of two eliminated bromine radicals (*vide infra*).

2.6.2. Laser Flash Photolysis. To further investigate the mechanism of the photoelimination reaction, nanosecond laser flash photolysis (LFP) experiments were performed on the compounds with the highest photochemical quantum yields, **PT-Br$_2$**, **PT-CN-Br$_2$**, **PT-CF$_3$-Br$_2$**, and **PT-C$_6$F$_5$-Br$_2$** (see Supporting Information for experiment setup and conditions).

The brominated compounds were excited within the low-energy absorption band using a 450 nm excitation pulse in the presence of DMBD under an argon atmosphere. The transient absorption (TA) spectrum of **PT-CF$_3$-Br$_2$** in the presence of ~0.2 M DMBD (3000:1 trap to tellurophene ratio) recorded at different times after the laser pulse displays intense absorption bands about 360 and 325 nm (Figure 7a). Similar features were observed in the TA spectra of the other three compounds (Figure S21, Supporting Information).

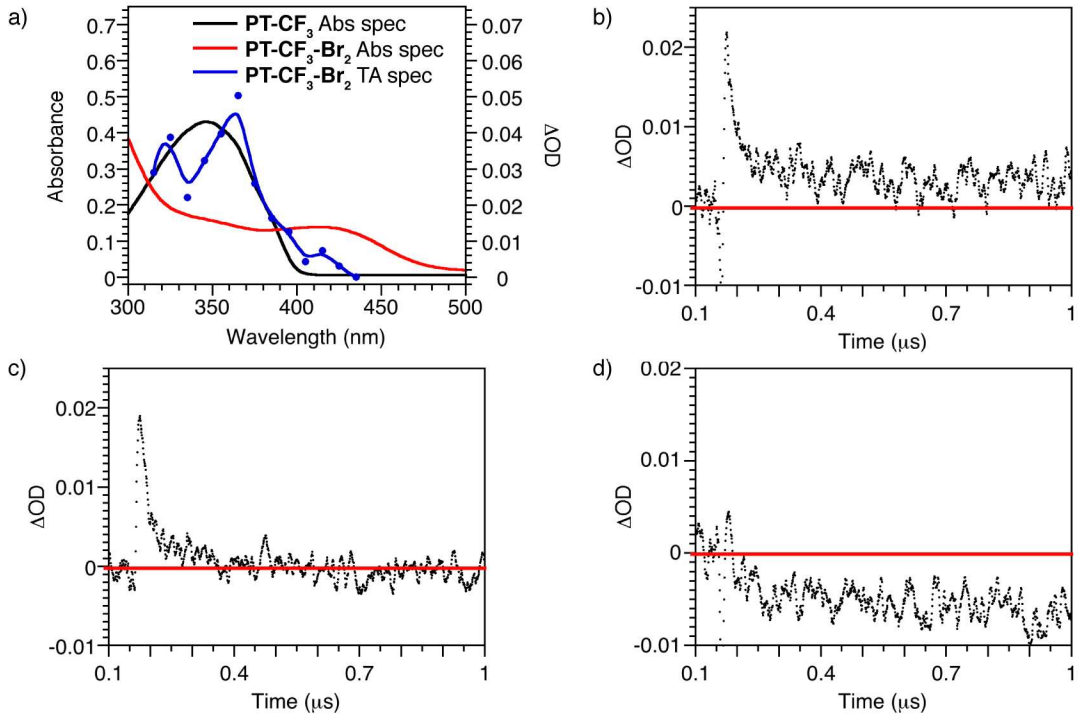

Figure 7. a) Optical absorption spectra of **PT-CF$_3$** and **PT-CF$_3$-Br$_2$** compared with the TA spectrum of **PT-CF$_3$-Br$_2$** in the presence of DMBD right after the 450 nm laser pulse; and single wavelength kinetic traces of $CHCl_3$ solutions of **PT-CF$_3$-Br$_2$** excited at 450 nm and monitored at (b) 388 nm, (c) 392 nm, and (d) 430 nm.

Single wavelength kinetic traces obtained at and about the low energy isosbestic point between the photoreactant (**PT-R-Br$_2$**) and the photoproduct (**PT-R**) were used to determine the nature of the observed transient species. Because the ground-state absorption of **PT-R** is greater than **PT-R-Br$_2$** at wavelengths shorter than the IP, the decay of a single wavelength trace to a final positive ΔOD is expected, confirming conversion of **PT-R-Br$_2$** to **PT-R**. On the other hand, at wavelengths longer than the IP, **PT-R** absorbs less than **PT-R-Br$_2$**, and a final negative ΔOD is expected. At the IP, the absorbance of the photoreactant and photoproduct is equal, thus they are silent in LFP and a final ΔOD of zero is expected. As a result, any signal observed in the kinetics trace could be attributed to the presence of a transient species. Single wavelength kinetic traces were collected at several wavelengths for **PT-CF$_3$-Br$_2$** (Figure 7b-d), **PT-Br$_2$**, **PT-CN-Br$_2$**, and **PT-C$_6$F$_5$-Br$_2$** (Figure S22, Supporting Information) in the presence of ~0.2 M DMBD. Indeed, the ΔOD monitored at the IP decays to zero after excitation, and in all cases a transient species with positive ΔOD is formed within the pulse of the laser (5-8 ns). Since this is the only active species at the IP, the decay can be used to determine the lifetime of the transient species, which is 20-70 ns for the different compounds (Table 3). Further discussion and a possible assignment of this transient will be presented below.

The IPs located by LFP are in good agreement with the IPs observed in the steady state optical absorption photolysis experiments with the exception of **PT-Br$_2$**. When probing the **PT-Br$_2$** sample at 386 nm (the IP determined during the steady state photolysis experiments), a final positive ΔOD is unexpectedly observed, while a final ΔOD of 0 is observed when probed at 398 nm. At the trap concentration used in these experiments, it is likely that this compound undergoes some amount of decomposition, which may explain the discrepancy observed, although a blue-shifted IP is usually observed when decomposition is present.

Table 3. Lifetimes of the transient species generated upon 450 nm excitation.

Sample	Monitored Wavelength (nm)	τ(ns)
PT-C_6F_5-Br_2 + DMBD	371	42.1 – 39.2
PT-CF_3-Br_2 + DMBD	390	45 – 42 – 39
PT-CN-Br_2 + DMBD	406	22.4 – 16.4 – 23.3
PT-Br_2 + DMBD	398	77.0 – 60.9

In order to assign the observed transient species and to gain insight into the photochemical mechanism, a series of experiments were performed. First, the possibility for triplet state formation due to the presence of the heavy atom tellurium was probed. Upon excitation of the non-brominated tellurophene **PT-CF_3** at 355 nm, an absorption band appears at 450 nm in the TA spectrum. The lifetime of this transient species is 1.3 μs and is attributed to absorption by the **PT-CF_3** triplet state. This is in agreement with the calculated absorption spectrum of the ground state triplet by DFT (Figure S23, Supporting Information). Interestingly, the TA spectrum and lifetime observed upon excitation of **PT-CF_3-Br_2** at 355 nm is different from the TA spectrum and lifetime obtained when **PT-CF_3-Br_2** is excited at 450 nm, which suggests that different transient species are formed under the different photolysis conditions. Furthermore, the TA spectrum and lifetime (1.3 μs) for **PT-CF_3-Br_2** are similar to those obtained for **PT-CF_3** when a 355 nm excitation is used (Figure 8), indicating that the same transient species is being observed in both samples. Since this transient was attributed to the **PT-CF_3** triplet, it follows that the dehalogenation process and excitation of the photoproduct must be complete within the pulse of the laser (5-8 ns). The **PT-CF_3** excited state singlet may then undergo intersystem crossing (ISC) to give the observed **PT-CF_3** triplet (Scheme S1, Supporting Information). This pathway cannot be accessed when a 450 nm laser pulse is used since the photoproduct does not absorb at this wavelength. Thus, the transient species with ~45 ns lifetime is observed under 450 nm excitation.

To further confirm the presence of triplet states, steady-state photoluminescence measurements of both **PT-CF$_3$** and **PT-CF$_3$-Br$_2$** were performed at low temperature (~ 77 K) under argon (Figure S24, Supporting Information). A phosphorescence band at 440 nm was observed for **PT-CF$_3$** (excitation at 355 nm), and two bands around 550 and 600 nm were observed for **PT-CF$_3$-Br$_2$** (excitation at 450 nm). Additionally, under O_2 atmosphere, both **PT-CF$_3$** and **PT-CF$_3$-Br$_2$** generate singlet oxygen ($^1O_2$) when they are excited at 355 and 450 nm, respectively. The $^1O_2$ quantum yield (Φ_Δ) approaches unity for **PT-CF$_3$** ($\Phi_\Delta \sim 1.0$) and is lower for **PT-CF$_3$-Br$_2$** ($\Phi_\Delta \sim 0.1$) in the absence of trap using *meso*-tetraphenylporphyrin (TTP) as a standard ($^{TPP}\Phi_\Delta \sim 0.66$ in CCl_4 and benzene).[67] Furthermore, **PT-CF$_3$** does not generate $^1O_2$ when irradiated at 450 nm, suggesting both **PT-CF$_3$** and **PT-CF$_3$-Br$_2$** generate $^1O_2$ from their respective triplet states. This evidence of **PT-CF$_3$-Br$_2$** triplet state formation suggests that ISC is competitive with bromine photoelimination.

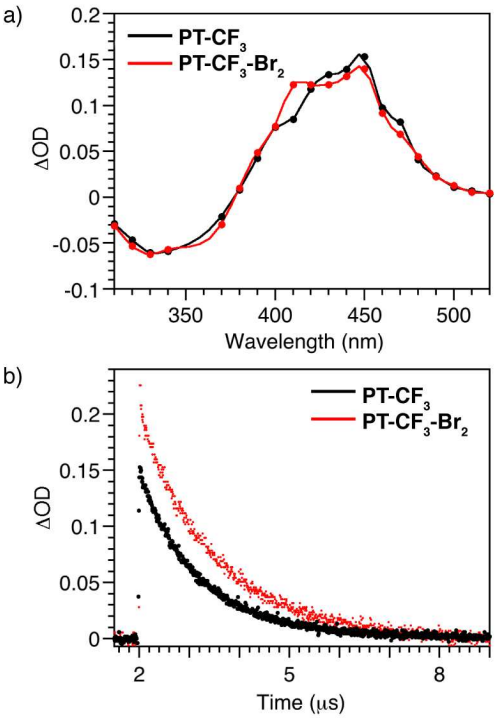

Figure 8. a) TA spectra and b) single wavelength kinetic traces (monitored at 410 nm) obtained for $CHCl_3$ solutions of **PT-CF_3-Br_2** and **PT-CF_3** containing DMBD upon irradiation at 355 nm under Ar atmosphere. Lifetime: ~ 1.3 μs.

As discussed above, halogen trapping experiments suggest that the bromine species generated upon photolysis is most likely $Br^{\bullet}$. However, direct detection of this species would be desired in order to fully characterize the photoelimination mechanism. Thus, it is important to identify a molecule that would react efficiently with $Br^{\bullet}$ yielding a readily detectable species. The reaction of bromide (Br^-) with bromine atoms ($Br^{\bullet}$) provides an ideal probe reaction, since the product ($Br_2^{\bullet-}$) absorbs strongly at 360 nm (ε_{360} = 9000 M^{-1} cm^{-1}).[68] Kinetic traces obtained upon excitation of solutions of **PT-C_6F_5-Br_2** and **PT-CF_3-Br_2** in the presence of tetraethylammonium bromide (TEABr, 3 mM) show a long lived intermediate (~9-12 μs) when monitored at the IPs (371 nm and 390 nm, respectively). Since these wavelengths coincide with the absorption of $Br_2^{\bullet-}$, the transient observed can be attributed to the formation of this intermediate. To further confirm this, TA spectra were recorded within 100 ns after excitation and compared to the TA spectra obtained for the solutions containing the DMBD trap. For both **PT-CF_3-Br_2** and **PT-C_6F_5-Br_2**, subtraction of the two spectra reveals an absorption band centered at 385 nm, attributed to absorption by $Br_2^{\bullet-}$ (Figure 9 and Figure S25, respectively). The same profile was found at various times after excitation. Thus, the absorption profile in the TA spectra and the long lifetimes support the formation of $Br_2^{\bullet-}$, which is further confirmation that photoelimination involves the release of bromine radicals (Scheme 3a).

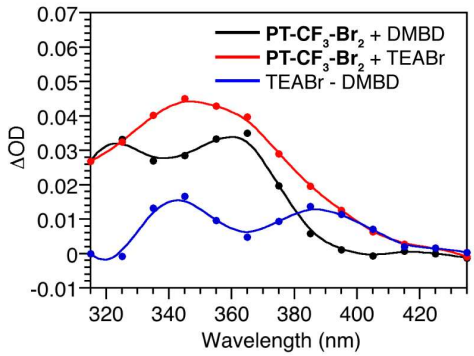

Figure 9. TA spectra of **PT-CF_3-Br_2** in the presence of DMBD and TEABr recorded within 100 ns after the laser pulse (450 nm) and the arithmetic subtraction of the two spectra.

In accordance with all of these results, plausible photochemical and photophysical mechanisms for both the non-brominated and brominated tellurophene systems can be described (Scheme 3b-c). Upon irradiation at 450 nm, **PT-R-Br_2** is excited to its very short lived singlet excited state (S_1; τ < 2 ns, no fluorescence emission detected), which is subject to either of the following competitive pathways: (a) intersystem crossing to the triplet excited state, T_1 (Path 1) followed by the concomitant relaxation to the singlet ground state (S_0) via radiative relaxation (phosphorescence, ~600 nm), non-radiative relaxation (Path 2), or by energy transfer to $^3O_2$ under aerobic conditions; *or* (b) photo-debromination via stepwise $Br^{\bullet}$ elimination (Path 3), which occurs within the time resolution of the instrument, and is confirmed by detection of $Br_2^{\bullet-}$ when LFP is carried out in the presence of TEABr (absorption at 380 nm with ~10 μs lifetime). The parent compounds (**PT-R**) can be excited using a 355 nm pulse and can undergo paths 1 and 2 explained above (labeled 1' and 2' in Scheme 3c), as well as generate $^1O_2$ under aerobic conditions.

Reasonable assignments for the ~50 ns transient species observed during LFP of the brominated compounds (Table 3) could be a) a photointermediate such as the monobrominated species **PT-**

R-Br$^{\bullet}$ formed after the first Br$^{\bullet}$ elimination, b) a singlet excited state of the photoreactant, or c) a triplet excited state of the photoreactant. The observation of the **PT-CF$_3$** triplet state (1.3 µs lifetime) upon excitation of **PT-CF$_3$-Br$_2$** at 355 nm, necessitates that dehalogenation, excitation of the photoproduct, and ISC all occur within the duration of the laser pulse (5-8 ns). Thus, the transient observed upon excitation at 450 nm cannot be assigned to a monobrominated intermediate, as this would be inconsistent with the fast dynamics upon excitation at 355 nm. Additionally, assignment of the transient to the singlet excited state can be discarded due to the lack of fluorescence emission. Thus, the ~50 ns transient is assigned to the **PT-R-Br$_2$** triplet state, the formation of which is competitive with the photoreaction, and is supported by the observation of phosphorescence and $^1O_2$ generation.

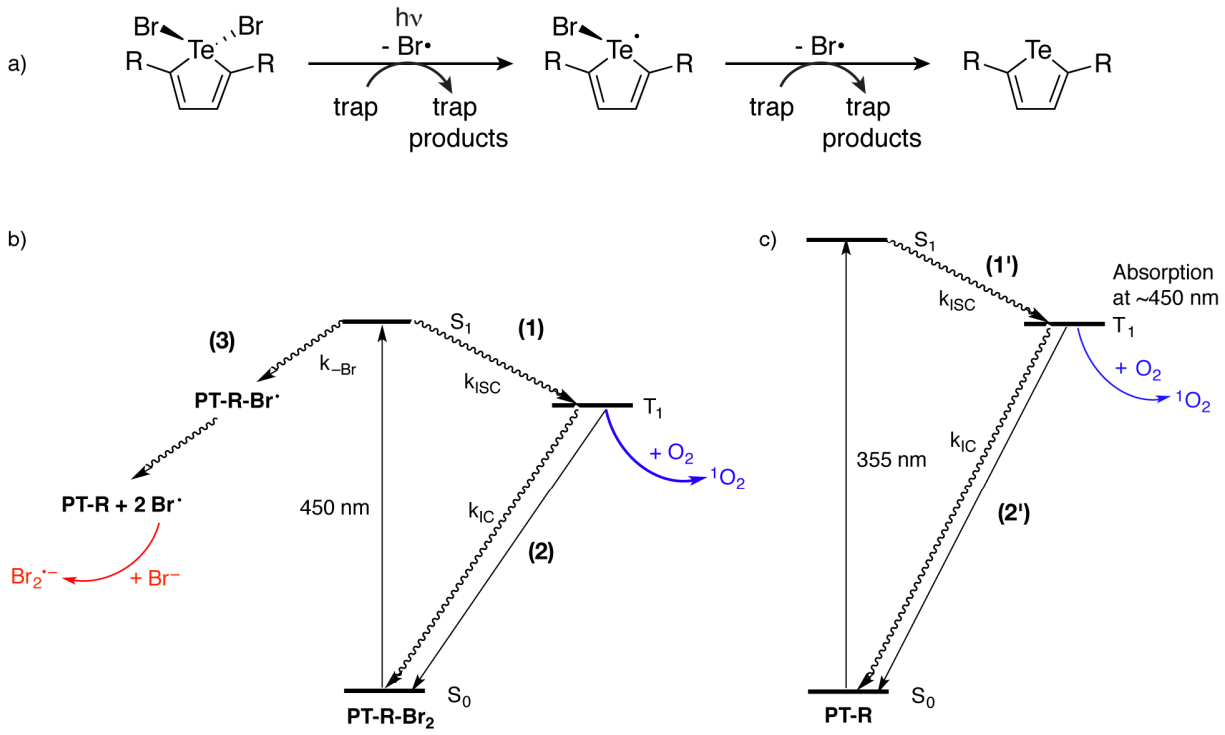

Scheme 3. a) Chemical mechanism of bromine photoelimination from **PT-R-Br$_2$**. b) Proposed photochemical and photophysical mechanisms for **PT-R-Br$_2$** upon excitation at 450 nm. c)

Proposed photophysics for **PT-R** upon excitation at 355 nm.

3. Conclusions

A series of substituted diphenyltellurophene compounds has been synthesized and the reactivity of these compounds has been evaluated in terms of oxidative addition and photoelimination of bromine. Density functional theory calculations support a dissociative mechanism for oxidative addition of Br_2 that involves the formation of an η^1-association complex, a monobrominated intermediate and finally the dibrominated product. Photoelimination of bromine is induced through excitation into the low-energy absorption band using blue or red LEDs. The photochemical quantum yield increases with increasing electron-withdrawing character of the substituents, with a value up to 42% achieved for the perfluorophenyl-substituted tellurophene at 5 M alkene trap concentration. The photoelimination reaction occurs from the S_1 excited state via elimination of two bromine radicals, confirmed by trapping experiments, however the photoreaction is competitive with intersystem crossing to the triplet state, as evidenced by the formation of singlet oxygen during photolysis under aerobic conditions. The results of these studies establish a mechanism for the efficient photoelimination of bromine from conjugated tellurophenes.

Supporting Information:

Experimental details, X-ray crystallography data, titration and photolysis data for all compounds, additional figures for DFT mechanistic study, GC-MS data, additional figures for LFP experiments, NMR spectra for all compounds, further discussion of trap products, and DFT optimized geometry coordinates and absolute energies.

Author Information:

Corresponding Authors:

*dseferos@chem.utoronto.ca
*scaiano@photo.chem.uottawa.ca

Notes:
The authors declare no competing financial interest.

Acknowledgments:

D. S. S. is grateful to NSERC, DuPont for a Young Professor Grant and the A. P. Sloan Foundation for a research fellowship in chemistry. E. I. C. is grateful to NSERC for a CGS D. We wish to acknowledge the Canadian Foundation for Innovation, Project Number 19119, and the Ontario Research Fund for funding of the Centre for Spectroscopic Investigation of Complex Organic Molecules and Polymers. We would like to thank Mark Taylor for the use of his GC-MS instrument. A. E. L. and J. C. S. thank the Natural Sciences and Engineering Research Council of Canada, the Canada Research Chairs Program and the Canadian Foundation for Innovation for generous support.

References:

(1) Hoffmann, N. *Chem. Rev.* **2008**, *108*, 1052–1103.
(2) Heyduk, A. F. *Science* **2001**, *293*, 1639–1641.
(3) Nocera, D. G. *Inorg. Chem.* **2009**, *48*, 10001–10017.
(4) Elgrishi, N.; Teets, T. S.; Chambers, M. B.; Nocera, D. G. *Chem. Commun.* **2012**, *48*, 9474–9476.
(5) Powers, D. C.; Hwang, S. J.; Zheng, S.-L.; Nocera, D. G. *Inorg. Chem.* **2014**, *53*, 9122–9128.
(6) Esswein, A. J.; Veige, A. S.; Nocera, D. G. *J. Am. Chem. Soc.* **2005**, *127*, 16641–16651.
(7) Cook, T. R.; Esswein, A. J.; Nocera, D. G. *J. Am. Chem. Soc.* **2007**, *129*, 10094–10095.
(8) Teets, T. S.; Lutterman, D. A.; Nocera, D. G. *Inorg. Chem.* **2010**, *49*, 3035–3043.
(9) Teets, T. S.; Nocera, D. G. *J. Am. Chem. Soc.* **2009**, *131*, 7411–7420.
(10) Cook, T. R.; McCarthy, B. D.; Lutterman, D. A.; Nocera, D. G. *Inorg. Chem.* **2012**, *51*, 5152–5163.
(11) Powers, D. C.; Chambers, M. B.; Teets, T. S.; Elgrishi, N.; Anderson, B. L.; Nocera, D. G. *Chem. Sci.* **2013**, *4*, 2880–2885.
(12) Cook, T. R.; Surendranath, Y.; Nocera, D. G. *J. Am. Chem. Soc.* **2009**, *131*, 28–29.
(13) Lin, T.-P.; Gabbaï, F. P. *J. Am. Chem. Soc.* **2012**, *134*, 12230–12238.
(14) Yang, H.; Gabbaï, F. P. *J. Am. Chem. Soc.* **2014**, *136*, 10866–10869.
(15) Hwang, S. J.; Powers, D. C.; Maher, A. G.; Anderson, B. L.; Hadt, R. G.; Zheng, S.-L.; Chen, Y.-S.; Nocera, D. G. *J. Am. Chem. Soc.* **2015**, *137*, 6472–6475.
(16) Karikachery, A. R.; Lee, H. B.; Masjedi, M.; Ross, A.; Moody, M. A.; Cai, X.; Chui, M.; Hoff, C. D.; Sharp, P. R. *Inorg. Chem.* **2013**, *52*, 4113–4119.
(17) Perera, T. A.; Masjedi, M.; Sharp, P. R. *Inorg. Chem.* **2014**, *53*, 7608–7621.
(18) Wickramasinghe, L. A.; Sharp, P. R. *Inorg. Chem.* **2014**, *53*, 1430–1442.

(19) Wickramasinghe, L. A.; Sharp, P. R. *J. Am. Chem. Soc.* **2014**, *136*, 13979–13982.
(20) Jahnke, A. A.; Howe, G. W.; Seferos, D. S. *Angew. Chem. Int. Ed.* **2010**, *49*, 10140–10144.
(21) Jahnke, A. A.; Seferos, D. S. *Macromol. Rapid Commun.* **2011**, *32*, 943–951.
(22) Jahnke, A. A.; Djukic, B.; McCormick, T. M.; Buchaca Domingo, E.; Hellmann, C.; Lee, Y.; Seferos, D. S. *J. Am. Chem. Soc.* **2013**, *135*, 951–954.
(23) Lee, W.-H.; Kyu Lee, S.; Suk Shin, W.; Moon, S.-J.; Kang, I.-N. *J. Polym. Sci. Part A: Polym. Chem.* **2013**, *51*, 2753–2758.
(24) Jung, E. H.; Bae, S.; Yoo, T. W.; Jo, W. H. *Polym. Chem.* **2014**, *5*, 6545–6550.
(25) Park, Y. S.; Kale, T. S.; Nam, C. Y.; Choi, D.; Grubbs, R. B. *Chem. Commun.* **2014**, *50*, 7964–7967.
(26) Park, Y. S.; Wu, Q.; Nam, C.-Y.; Grubbs, R. B. *Angew. Chem. Int. Ed.* **2014**, *53*, 10691–10695.
(27) Takimiya, K.; Kunugi, Y.; Konda, Y.; Niihara, N.; Otsubo, T. *J. Am. Chem. Soc.* **2004**, *126*, 5084–5085.
(28) Kaur, M.; Seul Yang, D.; Shin, J.; Wan Lee, T.; Choi, K.; Ju Cho, M.; Hoon Choi, D. *Chem. Commun.* **2013**, *49*, 5495–5497.
(29) Kaur, M.; Lee, D. H.; Da Seul Yang; Um, H. A.; Cho, M. J.; Kang, J. S.; Choi, D. H. *Chem. Commun.* **2014**, *50*, 14394–14396.
(30) Carrera, E. I.; Seferos, D. S. *Macromolecules* **2015**, *48*, 297–308.
(31) Rivard, E. *Chem. Lett.* **2015**, *44*, 730–736.
(32) Lapkowski, M.; Motyka, R.; Suwiński, J.; Data, P. *Macromol. Chem. Phys.* **2011**, *213*, 29–35.
(33) He, G.; Torres Delgado, W.; Schatz, D. J.; Merten, C.; Mohammadpour, A.; Mayr, L.; Ferguson, M. J.; McDonald, R.; Brown, A.; Shankar, K.; Rivard, E. *Angew. Chem. Int. Ed.* **2014**, *53*, 4587–4591.
(34) He, G.; Wiltshire, B. D.; Choi, P.; Savin, A.; Sun, S.; Mohammadpour, A.; Ferguson, M. J.; McDonald, R.; Farsinezhad, S.; Brown, A.; Shankar, K.; Rivard, E. *Chem. Commun.* **2015**, *51*, 5444–5447.
(35) Kryman, M. W.; Schamerhorn, G. A.; Yung, K.; Sathyamoorthy, B.; Sukumaran, D. K.; Ohulchanskyy, T. Y.; Benedict, J. B.; Detty, M. R. *Organometallics* **2013**, *32*, 4321–4333.
(36) Koide, Y.; Kawaguchi, M.; Urano, Y.; Hanaoka, K.; Komatsu, T.; Abo, M.; Terai, T.; Nagano, T. *Chem. Commun.* **2012**, *48*, 3091–3093.
(37) Kaur, M.; Da Seul Yang; Choi, K.; Cho, M. J.; Choi, D. H. *Dyes Pigm.* **2014**, *100*, 118–126.
(38) McCormick, T. M.; Carrera, E. I.; Schon, T. B.; Seferos, D. S. *Chem. Commun.* **2013**, *49*, 11182–11184.
(39) Annaka, T.; Nakata, N.; Ishii, A. *Organometallics* **2015**, *34*, 1272–1278.
(40) Mahrok, A. K.; Carrera, E. I.; Tilley, A. J.; Ye, S.; Seferos, D. S. *Chem. Commun.* **2015**, *51*, 5475–5478.
(41) Tsao, F. A.; Lough, A. J.; Stephan, D. W. *Chem. Commun.* **2015**, *51*, 4287–4289.
(42) Tsao, F. A.; Stephan, D. W. *Dalton Trans.* **2015**, *44*, 71–74.
(43) Tsao, F. A.; Cao, L.; Grimme, S.; Stephan, D. W. *J. Am. Chem. Soc.* **2015**, *137*, 13264–13267.
(44) Misra, S.; Chauhan, A. K. S.; Srivastava, R. C.; Butcher, R. J.; Duthie, A. *J. Organomet.*

Chem. **2015**, *791*, 119–123.
(45) Ali, A. M. M.; Ramazanova, P. A.; Abakarov, G. M.; Tarakanova, A. V.; Anisimov, A. V. *Russ. J. Gen. Chem.* **2015**, *85*, 770–772.
(46) Detty, M. R.; Luss, H. R. *Organometallics* **1986**, *5*, 2250–2256.
(47) Detty, M. R.; Friedman, A. E. *Organometallics* **1994**, *13*, 533–540.
(48) Detty, M. R.; Friedman, A. E.; McMillan, M. *Organometallics* **1994**, *13*, 3338–3345.
(49) McCormick, T. M.; Jahnke, A. A.; Lough, A. J.; Seferos, D. S. *J. Am. Chem. Soc.* **2012**, *134*, 3542–3548.
(50) Carrera, E. I.; McCormick, T. M.; Kapp, M. J.; Lough, A. J.; Seferos, D. S. *Inorg. Chem.* **2013**, *52*, 13779–13790.
(51) Carrera, E. I.; Seferos, D. S. *Dalton Trans.* **2015**, *44*, 2092–2096.
(52) Detty, M. R. *Organometallics* **1991**, *10*, 702–712.
(53) Aprile, A.; Iversen, K. J.; Wilson, D. J. D.; Dutton, J. L. *Inorg. Chem.* **2015**, *54*, 4934–4939.
(54) Vilhelmsen, M. H.; Jensen, J.; Tortzen, C. G.; Nielsen, M. B. *Eur. J. Org. Chem.* **2012**, *2013*, 701–711.
(55) Mack, W. *Angew. Chem. Int. Ed.* **1966**, *5*, 896–896.
(56) Terao, Y.; Wakui, H.; Satoh, T.; Miura, M.; Nomura, M. *J. Am. Chem. Soc.* **2001**, *123*, 10407–10408.
(57) Terao, Y.; Wakui, H.; Nomoto, M.; Satoh, T.; Miura, M.; Nomura, M. *J. Org. Chem.* **2003**, *68*, 5236–5243.
(58) Peng, C.; Schlegel, H. B. *Isr. J. Chem.* **1993**, *33*, 449–454.
(59) Peng, C.; Ayala, P. Y.; Schlegel, H. B.; Frisch, M. J. *J. Comput. Chem.* **1996**, *17*, 49–56.
(60) Fukui, K. *Acc. Chem. Res.* **1981**, *14*, 363–368.
(61) Parker, C. A. *Proc. R. Soc. London, Ser. A* **1953**, *220*, 104–116.
(62) Hatchard, C. G.; Parker, C. A. *Proc. R. Soc. London, Ser. A* **1956**, *235*, 518–536.
(63) Kuhn, H. J.; Braslavsky, S. E.; Schmidt, R. *Pure Appl. Chem.* **2004**, 2105–2146.
(64) Tzerpos, N. I.; Zarkadis, A. K.; Kreher, R. P.; Repas, L.; Lehnig, M. *J. Chem. Soc., Perkin Trans. 2* **1995**, 755–761.
(65) Clennan, E. L.; Chen, X. *J. Am. Chem. Soc.* **1989**, *111*, 5787–5792.
(66) Anderson, J. E.; Doecke, C. W.; Pearson, H. *Journal of the Chemical Society, Perkin Transactions 1* **1976**, *1976*, 336–341.
(67) Wilkinson, F.; Helman, W. P.; Ross, A. B. *J. Phys. Chem. Ref. Data* **1993**, *22*, 113–262.
(68) Scaiano, J. C.; Barra, M.; Krzywinski, M.; Sinta, R.; Calabrese, G. *J. Am. Chem. Soc.* **1993**, *115*, 8340–8344.

TOC:

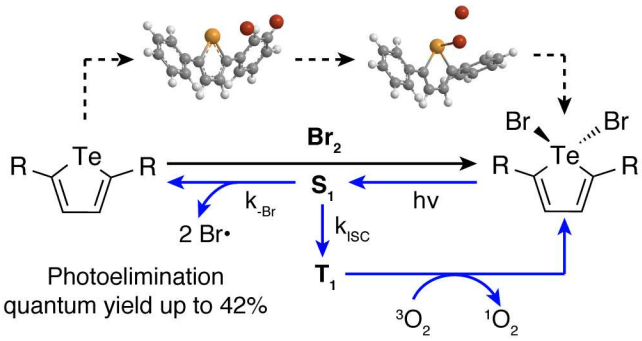
R
Te
R
Br2
S1
hv
Br
Br
R
Te
R
k-Br
2 Br•
kISC
T1
3O2
1O2
Photoelimination
quantum yield up to 42%